LBNL-44329
Preprint

ERNEST ORLANDO LAWRENCE BERKELEY NATIONAL LABORATORY

Marine Magnetotellurics for Base Salt Mapping: Gulf of Mexico Field-Test at the Gemini Structure

G. Michael Hoversten, Steve Constable, and H. Frank Morrison

Earth Sciences Division

September 1999

Submitted to
Geophysics

REFERENCE COPY
Does Not
Circulate
Bldg. 50 Library - Ref.
Lawrence Berkeley National Laboratory

LBNL-44329
Copy 1

DISCLAIMER

This document was prepared as an account of work sponsored by the United States Government. While this document is believed to contain correct information, neither the United States Government nor any agency thereof, nor the Regents of the University of California, nor any of their employees, makes any warranty, express or implied, or assumes any legal responsibility for the accuracy, completeness, or usefulness of any information, apparatus, product, or process disclosed, or represents that its use would not infringe privately owned rights. Reference herein to any specific commercial product, process, or service by its trade name, trademark, manufacturer, or otherwise, does not necessarily constitute or imply its endorsement, recommendation, or favoring by the United States Government or any agency thereof, or the Regents of the University of California. The views and opinions of authors expressed herein do not necessarily state or reflect those of the United States Government or any agency thereof or the Regents of the University of California.

LBNL-44329

Marine Magnetotellurics for Base Salt Mapping: Gulf of Mexico Field-Test at the Gemini Structure

G. Michael Hoversten, Steve Constable, and H. Frank Morrison

Earth Sciences Division
Ernest Orlando Lawrence Berkeley National Laboratory
University of California
Berkeley, California 94720

September 1999

This work was supported by the Director, Office of Science, Office of Laboratory Research, of the U.S. Department of Energy under Contract No. DE-AC03-76SF00098.

Marine Magnetotellurics for Base Salt Mapping: Gulf of Mexico Field-Test at the Gemini Structure

*Presented, 1998 SEG annual meeting.

G. Michael Hoversten, Lawrence Berkeley National Laboratory

Steve Constable, Scripps Institution of Oceanography

H. Frank Morrison, University of California at Berkeley

ABSTRACT

A seafloor magnetotelluric (MT) survey was conducted over the Gemini subsalt petroleum prospect in the Gulf of Mexico, to demonstrate that the base of salt can be mapped using MT methods. The high contrast in electrical resistivity between the salt and the surrounding sediments provides an excellent target for MT. The Gemini salt body is located at 28\deg 46' N 88\deg 36' W. It is a relatively complex shape buried 2 to 5 km below the seafloor in 1 km deep water. Its geometry has been previously determined using 3D seismic pre-stack depth migration with well log control. In order not to confuse limitations in interpretation technique with limitations in data acquisition, numerical forward and inverse modeling guided the survey design to locate a profile that would be amenable to 2D inversion, even though the body was clearly 3D. Data were collected using autonomous seafloor data loggers equipped with induction coil magnetic sensors and electric field sensors consisting of silver-silver chloride electrodes connected to an AC-coupled amplifier originally designed for seafloor controlled source studies Nine sites of excellent quality MT responses were obtained. Smooth 2D inversion of the data produce a confined resistive anomaly at the correct location and depth, and recently developed sharp boundary 2D inversion recovers base of salt in excellent agreement with

the seismic models. Simple perturbation analysis shows that base salt has been resolved to within 5-10% of burial depth.

INTRODUCTION

The magnetotelluric (MT) method has been used for many decades on land to assist in exploration for petroleum (Vozoff, 1972 and Orange, 1989). It is particularly useful for basin reconnaissance, and in areas where seismic methods perform poorly, such as carbonate and volcanic terrain. In areas where sediments are obscured by rock units that scatter and reflect most normal incident seismic energy, electrical methods may be very helpful in determining the structural relationships and thickness of the various units. It is generally true that rocks with high seismic velocities and impedance contrasts are also higher in electrical resistance than surrounding sediments.

For these reasons, Hoversten and Unsworth (1994) and Hoversten et al. (1992) carried out model studies to test the feasibility of using MT methods to map base of salt in the Gulf of Mexico (GOM) and other regions. Salt has a high acoustic contrast with surrounding sediments which makes seismic methods difficult, and it is much more resistive than water saturated clastic sediments. It was shown that with MT data of reasonable quality in the 1 s to 1000 s band, base of salt could indeed be mapped with accuracy approaching that of seismic methods. Unfortunately, however, most marine MT up to that time involved use of long period instrumentation in deep ocean waters, probing Earth's mantle at depths of 100 km and deeper (e.g. Filloux, 1983). It was generally believed that attenuation of the natural EM fields by seawater precluded the use

of MT in the ocean at any significant depth (Chave et al. 1991). An early attempt to use MT in very shallow water in the GOM met with limited success (Hoehn and Warner, 1960), however data processing techniques at the time were unable to remove the large wave motion noise resulting from the experiments depth of only 10m. In addition the equipment was far too bulky to be commercially viable. And because it was a moored system it would not have been practical in modern prospects where the seafloor depth approaches 2000 m. Traditionally, controlled source methods have been used on the seafloor to replace the EM energy lost in the seawater (e.g. Constable and Cox, 1996), and have been proposed for offshore exploration (Constable et al., 1986).

To overcome the limitations of the existing marine MT method, Constable et al. (1998) developed a new generation of marine instrumentation, capable of detecting and amplifying the weak seafloor electromagnetic signals in the band needed to map continental shelf structures. A single test deployment off San Diego, California in 1995 produced good quality data on the first attempt, and so in 1996 field trials were carried out in the GOM over both the Mahogany and Gemini sub-salt discoveries, to develop second-generation equipment capable of frequent and repeated deployment. Excellent quality electric field records were collected from the new instruments, but early efforts to record magnetic field data were frustrated both by instrument motion in the Earth's large magnetic field and by magnetic noise generated by fluctuating power consumption of the nearby logging electronics. To address these problems, logging software and hardware were modified to maintain constant power consumption and the instrument anchor increased from 75 to 200 kg. These changes improved the quality of the magnetic data

considerably, and this current paper describes results from a second survey over the Gemini prospect in 1997, designed explicitly to show the power of the marine MT method to map base salt economically with a small number of seafloor stations. The following sections describe the equipment, survey design, data acquisition and processing, inversion and sensitivity analysis.

SEAFLOOR MT SYSTEM

Constable et al. (1998) give a detailed description of the MT system and the 1995 offshore California test. The seafloor MT instrument is an autonomous data logging package that free-falls to the seafloor under the weight of an anchor that is later released, to allow the otherwise buoyant package to float back to the surface. While a moored system might be more reliable and even collect better quality data, the free vehicle approach has a big advantage in the time taken to deploy and recover the system, especially in deep water. The ship is not encumbered during the time it takes the instrument to sink to or rise from the seafloor, and so many instrument systems can be deployed to record simultaneously, which not only increases productivity, but allows advantage to be taken of modern array-based processing schemes (e.g. Egbert, 1997).

The seafloor instrument is a modular package composed of a digital data logging system, an acoustic navigation/release unit, electric and magnetic field sensors, glass flotation balls, and concrete anchor, all held together by a largely plastic frame. If the electric and magnetic sensors are replaced by hydrophones, the system can, and has, performed double-duty as a seafloor seismic recorder. The logging system stores 16-bit

data to magnetic disk, and is limited in capacity only by the size of available disk drives, currently 18 GByte. The unit is presently being upgraded to 24-bit capability. The magnetic sensors are commercially available induction coils with an operating band from 10,000 s to 1000 Hz, housed in an aluminum pressure case. The conductive pressure case acts as a high-cut filter with a corner frequency around 1 Hz. It is the electric field sensors, based on the seafloor controlled source EM system described by Webb et al. (1985) and Constable and Cox (1996), that sets this instrument apart from its predecessors and long-period cousins. Silver-silver chloride electrodes are capacitively coupled to a low-noise chopper amplifier with gain of 1,000,000. The electrodes are mounted on the ends of four orthogonal plastic arms 5 m long. Figure 1 shows the signal to noise relationships for this amplifier/electrode system, collected by taping electrodes close together and deploying an instrument in 100 m water in the GOM (figure 5 of Constable et al., 1998, used an indirect estimate of the noise characteristics which overestimated the noise level).

The compact design means that the instrument is relatively light (about 150 kg without anchor), and can be airfreighted to the survey location. However, it also means that the magnetic sensors are very close to the data logging system and will detect variations in logger power consumption as magnetic noise. Consequently, it was found that the logger CPU clock speed could not be cycled to reduce overall power consumption, and so the instrument consumes a relatively high 250 mW, to which the two commercial induction coils add another 300 mW for 550 mW total. However, this is still low enough for the instrument to operate for nearly a week from rechargeable

batteries and over a month from lithium batteries. The current version of the logger has a disk drive interface within the pressure cap, allowing the contents of the disk drive to be recovered without opening the pressure case. This improves both the reliability of the instrument and speed of redeployment.

To synchronize instrument recordings between seafloor units and with land remote reference stations, an on-board crystal oscillator with a drift rate of 1 ms per day is set to GPS time at the start and end of each deployment. The sample rate is typically 25 Hz, and deployment duration is between 18 and 48 hours which, depending on conditions, allows MT response functions to be computed between 10 Hz and 1,000 to 10,000 s period. An example of data collected during the 1997 survey is shown in figure 2.

EXPERIMENT DESIGN FOR THE GEMINI SALT STRUCTURE

Figure 3 is a 3D rendering of the Gemini salt structure, using the top and base picks from the 3D seismic data provided by Chevron. Previous model studies (Hoversten et al. 1998) showed that the MT method is insensitive to the resistivity of the salt body, because once the salt becomes about 10 times more resistive than the surrounding sediments induced currents are effectively excluded from the salt and the MT response 'saturates'. Similarly, conductive inhomogeneities within the salt have little or no effect on the response. Thus, our experiment is sensitive only to the salt geometry. The top and base salt picks from seismic were use to construct a 3-D finite difference numerical model of the resistivity for calculating the MT response of the structure (Mackie et al. 1993). The 3D numerical model used for experiment design incorporated 1 km of seawater over the prospect. The salt bodies were assigned a resistivity of 100 ohm-m and

were embedded in a uniform 0.5 ohm-m sediment halfspace. The 0.5 ohm-m was a reasonable near-worst case (small skin depths) to conservatively represent the frequencies that would be required. The salt resistivity of 100 Ω-m represents a contrast with the sediments of 200 to 1 so that the MT response is effectively independent of the salt resistivity. The numerical MT response was used in the experiment design phase to determine the sensitivity of the MMT data to the base of the salt and to choose a profile amenable to 2D inversion with a limited number of sites. At this stage it was important to image the base of the salt without being limited by interpretation techniques, which at the time were largely limited to 2D inversion and 3D forward modeling. It was important to demonstrate the viability of the MT method, and not to confuse our inability to invert 3D data with our ability to collect high quality MT data that were sensitive to salt geometry. Figure 4 shows plan views of the Zxy (E field east-west and H field north-south) and Zyx (E field north-south and H field east-west) apparent resistivities at 1000s (0.001 Hz) and 100s (0.01 Hz) periods along with the survey line. The orientation of the apparent resistivity (and phase) anomalies coincides with that of the salt structure. The 500m salt isochron map with the survey line is shown in figure 5. The survey line was chosen to be orthogonal to the local strike of the structure thus allowing the impedance calculated using E in-line and H orthogonal to the line to be defined as the TM mode for 2D inversions.

At the time of the experiment design phase the Sharp Boundary Inversion (SBI), Smith et al. (1999), algorithm was not yet available so all inversion tests were done using the smooth Occam 2D inversion of deGroot-Hedlin & Constable (1990). Inversion tests on the numerical data showed that data in the frequency band between 0.1 and 0.01 Hertz were critical to resolve the base of the salt. Additional numerical tests showed that 2D inversion of the data should provide reasonable accuracy on the base salt.

The three-dimensional modeling of the Gemini salt guided the placement of the survey line that ran nearly N45E as shown in figures 4 and 5. At the southwest end of the line the salt is very thin (<300m) and deep (5km). In the middle, beneath sites 10-12, the salt thickens to approximately 2 km and terminates just NE of site 12.

DATA ACQUISITION AND PROCESSING

The survey was conducted with two land reference sites for the remote-reference processing (Gamble et al. 1978). The remote sites were near Thibodoux, LA and Alexandria, LA. A total of 46 deployments were made at 22 sites along the 2D profile, with 45 deployments recovering data. However, about the first half of the deployments had high noise levels in the magnetic recordings, which was remedied during the survey by altering the software and clock speed of the acquisition CPU. Also, in order to isolate noise problems such as this, electric and magnetic sensors were deployed separately on different instruments (we have since demonstrated the ability to collect coincident electric and magnetic data of good quality from a single instrument).

Separate electric and magnetic sensor deployments were combined from the second half of the survey to yield 9 sites of excellent quality along a profile, shown as black filled circles in figure 5. The 200kg anchors employed in the 1997 survey and modified system electronics resulted in greatly improved magnetic field data. Recording times were on the order of 24 hours at each site with some variations due to the logistics of multiple deployments and recoveries.

The data were processed using the "robust" multi-station MT processing algorithms of Egbert (1997). This processing not only reduces outlier populations but also takes advantage of all simultaneous recordings to produce improved impedance estimates. Overall data quality in the 0.003 to 1.0 Hz band was excellent and comparable to land data surveys. Figures 6 and 7 show apparent resistivity and phase data respectively for the 9 seafloor sites shown in figure 5. The data in figures 6 and 7 are rotated so than the X-axis is north and the Y-axis is east. A selection of impedance polar diagrams is plotted in figure 8. The magnitude of the off-diagonal elements of the impedance tensor is plotted in black as the impedance tensor is rotated through 360 degrees, the magnitude of the on-diagonal elements is shown in red with the angle of the maximum in the off-diagonal elements shown as green line from the origin. The polar diagrams show that at high frequencies the response is nearly 1D (off-diagonal magnitudes circular, on-diagonals nearly zero) and in the mid-frequencies the response in nearly 2D with the orientation of the magnitude of the off-diagonals in a north-east south-west direction and the on-diagonals nearly zero. At the lowest frequencies the responses become more 3D in nature (large on-diagonal elements). At sites on either side of the crest of the salt where the salt is either not present or is thin and deep the polar diagrams retain their 1D nature to lower frequencies.

2D INVERSIONS OF GEMINI MMT DATA

In order to test the relative performance of algorithms and also to provide enhanced confidence in the information content of the data, we used four different 2D MT inversion algorithms on the data. They are; 1) Smith & Booker (1988); 2) a non-

linear conjugate gradient (NLCG) algorithm, Mackie et al. (1997); 3) the Occam 2D algorithm, deGroot-Hedlin & Constable (1990); and 4) the Sharp Boundary Inversion algorithm, Smith et al. (1999).

All data used in 2D inversions were rotated so that the Z_{xy} impedance had E_x oriented along the line direction. This rotation was consistent with the line being perpendicular to strike as shown by the polar diagrams (figure 8). The Z_{xy} impedance was defined as TM for 2D inversion of the data. Previous numerical modeling of conductive bodies, Wannamaker et al. (1984), and of salt structures, Hoversten et al. (1998), showed that 2D inversions of potential 3-D data are most accurate if only the TM mode is used. Therefore, all inversions of the Gemini data used only the TM mode in the frequency range from 1 to 0.001 Hertz.

The first three algorithms listed above find models that are smooth both vertically and horizontally. They were all started from a 0.7 ohm-m halfspace with no a priori information used as constraints. Figure 9 shows the 2D inverse model produced by the RRI algorithm of Smith & Booker (1988). The version of RRI algorithm we used did not incorporate the seawater. The effects of the conductive seawater are only significant when resistive structure is near surface and acts to force currents up into the water. In this case these effects were not significant. Figure 10 shows the inverse model produced by the NLCG algorithm of Mackie et al. (1997). The inverse model from the Occam 2D algorithm will be considered later. All of the smooth inversions provided consistent model results in the upper 5 km. All showed the presence of resistive (> 1Ω-m) material

just below the seafloor, all had a sharp increase in resistivity that corresponded with the top salt as picked from the 3-D seismic and all showed a zone just above salt that had lower resistivity than seawater. Finally, all showed the salt to be have a base dipping to the south-west roughly parallel to its top down to a depth of approximately 5 km.

The fact that three different algorithms gave very similar pictures in the upper 5 km and that they indicated the presence of a confined salt body in the correct location was reassuring. However, the smooth inversions provide a fuzzy base salt picture, and to pick the location of a presumably sharp boundary a particular contour of the smooth inverse model resistivities must be chosen using test inversions of forward numerical model data. As shown in Smith et al. (1999) the resistivity contour of smooth inverse models which corresponds to a sharp resistivity contrast (interface) changes as a function of the depth of the interface. So that as a resistivity interface becomes deeper a lower value of the contour of a smooth inverse model will correspond to its true depth. In order to improve the resolution of the base salt we made use of some of the constraining features possible with the Occam 2D algorithm and used the SBI algorithm in our final inversions.

We assumed that the location of the top of salt was accurately known from the seismic data. The Occam 2D inversion shown in figure 11 had the smoothing constraints eliminated at the known location of the top salt. This allows the algorithm to place high resistivity salt next to low resistivity sediments at the top salt boundary. When smoothing is done across the top salt boundary, the result is to push more resistive

material to greater depths to accommodate the lack of higher resistive material at the top of salt, thus degrading the base salt image.

The 2D SBI, Smith et al. (1999), inversion is parameterized to accommodate sharp contrasts in resistivity across boundaries and thus eliminates some of the ambiguity in interpreting smooth inverse models. Rather than parameterizing the model in terms of blocks of unknown resistivity, the SBI parameterizes the model in terms of boundaries between layers and resistivities of the layers. The layers can be parameterized by either the thickness of the layers or by the depths to the interfaces between each layer. The boundaries are defined by nodes superimposed on the underlying finite element grid used for calculations of the responses. The resistivities are defined laterally at the node locations and are constant vertically within each layer. The resistivities vary linearly between nodes in the horizontal direction within each layer. In order to stabilize the inversion a smoothing constraint is placed on the interface depths or layer thickness and on the horizontal variation of resistivity. At each iteration the layer resistivities are projected onto an underlying finite element mesh for the MT calculations.

Figure 12 shows the SBI model, parameterized in layer thickness, for the Gemini data. The calculated apparent resistivity and phase for this model shown in figure 12 are overlaid on the data in figures 13 and 14 respectively. Because data variance estimates were unrealistically low we assigned an error floor of 5% on all data used for inversion. The error bars shown in figures 13 and 14 are from the processing and show that the frequency to frequency scatter is often greater than the estimated error. With the error

floor set at 5% the RMS misfit for the SBI inverse model was 2.4. The majority of the misfit comes from the systematic bias in the phase. The calculated phase tracks the shape of the observed phase but is generally low at every site. The cause of this phase bias is unknown at this time.

Because the SBI is parameterized by layer boundaries a starting model with the appropriate number of layers is required. In this case the results from the smooth inversions were used as a guide in building the SBI starting model. In particular, a near-surface resistive layer was indicated. The presence of a deeper resistive layer was indicated in the apparent resistivity curves at lower frequencies and in the smooth inversions. The starting location of the base salt was deep enough to encompass the high resistive zone shown on all the smooth inversions.

Nodes beneath the observation sites parameterized each layer. Additionally, a node was added between sites 13 and 14 to better describe the crest of the salt on the top boundary, and a node was added between sites 12 and 14 to describe the edge of the salt. Beyond site 12, where the seismic data showed no salt, the base salt layer was moved to coincide with the top salt and its location was fixed, effectively eliminating the salt layer to the northeast of site 12. The near-surface resistive (relative to the underlying sediment) layer was set at a constant thickness and only its lateral resistivity was allowed to vary. Because the top of salt was well determined by the seismic data its location was fixed in the inversion.

One of the features of the SBI is the ability to fix, constrain or link parameters in the inversion. All these serve to reduce the possible variations in the model. The thickness of the salt layer was constrained to be within 100% of its starting values. This would allow the salt thickness to be between 0 and 16 km. The sediment resistivities beneath the salt and the resistivities in the deepest (more resistive) layer were linked together so that these layers had constant resistivities laterally. In addition, the salt resistivity was fixed at 10 Ω-m. This is justified because the MT response saturates as the resistivity of a body becomes greater than 10 to 20 times that of the background. In the GOM bulk salt resistivities are more than 20 times the background sediment resistivities and for the skin depths of interest the MT response is totally governed by the distortion of electric currents in the sediments around the resistive salt. There is no contribution from induced currents within the salt. These constraints greatly reduced the number of parameters needed in the inversion.

The SBI, parameterized in layer thickness, placed a base salt interface within a few percent of the 3-D seismic pick down to a depth of 5km. In addition to the base salt the inversions of the data indicated the presence of a deep resistive zone which could correspond to Cretaceous sediments or carbonates. The experiment was not designed to acquire accurate low frequency data. In addition, data sampling restricted to a single line does not permit examination of the lateral structural variation. Longer recording times to improve data quality below 0.001 Hertz and seafloor sampling on a regular grid would be required to derive information about the deeper structure.

While the match between the base salt inversion results from the SBI and the seismic base salt pick shown in figure 12 is exciting it must be remembered that the choice of regularization imposes a bias on the resulting inverse model. In particular, the SBI shown in figure 12 was parameterized in terms of the thickness of the layers. This means that the regularization, or smoothing constraint, produces the smallest contributions to the object function by having layers with a minimum variation in thickness. The salt shown in figure 12 has nearly constant thickness, slightly thicker near the crest and slightly thinner at depth.

In order to demonstrate the effects of the choice of regularization on the final model we used the 3D numerical model from the experiment design (salt structure shown in figure 3, data shown in figure 4) and added a resistive basement at a depth of 8 km. The numerical data between 0.001 and 0.1 Hz was used in SBI inversions where the starting model was identical to that used in figure 12. Only the lower frequencies were used since the object is to illustrate the effects on the base salt and deep resistive structure. Two SBI inversions were run, one parameterized by layer thickness and the other parameterized by layer interface depth. In the second case the regularization favors models with a layer boundary of smooth (constant) depth. Both inversions assumed 5% noise and were run to a RMS data misfit of 1.0. Figures 15 and 16 show the final inverse models for the thickness and depth parameterizations respectively.

The resemblance between figures 12, the field data inversion and figure 15, the numerical model data inversion, is striking. The thickness of salt in the inverse model at

the beginning of the line where the salt is deep is due to the thickness parameterization. Comparing figures 15 and 16 we see that if the model is parameterized in depth, the salt is thinned to almost zero. The effect on the deep resistor is also significant. While the deep resistor is flat at a depth of 8km the thickness inversion has produced roughly 2km of relief on this interface by keeping the thickness of the overlying sediments roughly constant.

Using only the SBI inverse in isolation one could not choose between the two possible SBI models. However, when the two SBI models are compared to the smooth inverse models (particularly the Occam2D model that incorporated a sharp contrast at the top of salt) the SBI thickness model can be selected as the preferred interpretation since it is more consistent with the smooth models. The SBI depth model can be taken as a warning that the salt thickness at the beginning of the line where it is deepest, can be anywhere between zero and 1km thick.

SENSITIVITY OF MMT DATA TO VARIATIONS IN BASE SALT DEPTH

As we have seen from comparing the depth and thickness inversions of the 3D numerical data two models with significant differences can be found which both fit the data equally well. In the case of the thickness parameterization, figure 15, the maximum error in the base salt is at the beginning of the line where the salt is thinnest and is about 1km at a depth of 5km, or 20%. In the case of the depth parameterization, figure 16, the maximum error in the base salt occurs below the crest of the salt and is about 1km at a

depth of 4km or about 25%. These maximum errors are localized laterally so that the average error on the base salt depth is about 7% for both examples.

In order to access the sensitivity of TM mode MMT data to changes in the Gemini base salt depth (for the preferred model parameterized by layer thickness) the 2D model derived from the SBI inversion, figure 12, was modified by adding and subtracting 300m of salt from the base. The percent change in apparent resistivity from the initial model at sites 5 and 11 is shown in figure 15. Site 5 is over the deepest and thinnest section of salt while site 11 lies above the crest of the shallowest and thickest salt. Changing the base salt by 300m produces a 10% change at site 11 and a 6% change at site 5. The phase data is similarly affected.

These tests indicate that variations of 300m (or approximately 5% of depth at the deepest salt locations) in the base salt depth would produce changes in the data which should be detectable in the field data. However, as the SBI inversions of the 3D numerical model data demonstrate, maximum errors of up to 25% can occur in the estimated depth to base of salt at certain locations.

CONCLUSIONS

The 1997 Gulf of Mexico MMT survey described in this paper represents the first successful work of its kind. The project was a success both in terms of high quality seafloor MT data acquisition and in terms of a successful interpretation of the resulting data. The inverse models, which fit the observed data, are of sufficient fidelity to answer

significant exploration questions regarding the shape and location of base salt structures. The use of the top of salt interface provided by seismic data contributes greatly to the resolution of the base of the salt by the MMT. The technique has application worldwide, not only for base salt mapping but also for mapping base of carbonates and basalt.

The choice of model parameterization and regularization strongly effect the resulting inverse models produced. This is clearly demonstrated by comparing the four inverse models, which fit the field data, as well as comparing the two SBI inverse models that fit the 3D numerical data. While the SBI reduces some ambiguity inherent in picking a sharp contact from a smooth model such as those produced by Occam 2D inversions, it has its own inherent ambiguities based on the choice of parameterizing layers by their thickness or their depths. In producing a final interpretation of MMT data an interpreter must still synthesize the results of multiple inversions, forward modeling (2D and 3D), and basic geologic knowledge to come up with a most likely scenario.

While the experiment was not designed to look deeper than the base of salt at Gemini, the resulting inverse models offer the tantalizing potential of providing information of the deeper structure of the Gulf. The technology is moving into commercialization. Two commercial surveys were conducted in the GOM in the summer of 1998.

ACKNOWLEDGEMENTS

The authors are grateful to the Marine MT Consortium for their support and for the support of the Director, Office of Science, Office of Laboratory Research, of the U.S. Department of Energy, under Contract No. DE-AC03-76SF00098. The consortium membership at the time of acquisition and processing of the data included AGIP, Anadarko Petroleum, BP, BHP, British Gas, Chevron, Texaco and Baker Atlas.

The authors would also like to thank Mary Ann Mulrey and Ransom Reddig of AOA Geophysics and Clark Scott and Diane Gievers of Engineering Geoscience UC Berkeley for their work in data acquisition and processing.

REFERENCES

Chave, A. D., Constable, S. C. and Edwards, R. N., 1991, Electrical exploration methods for the seafloor, in Nabighian, M. N., Ed., Electromagnetic methods in applied geophysics, 2: Soc. Expl. Geophys., 931-969.

Constable, S. C., Cox, C. S. and Chave, A. D., 1986, Offshore electromagnetic surveying techniques: 56th Annual Internat. Mtg., Soc. Expl. Geophys., Expanded Abstracts, Session:EM3.1.

Constable, S., and C., S., Cox, 1996, Marine controlled source electromagnetic sounding 2. The PEGASUS experiment: J. Geophys. Res., **101**, 5519-5530

Constable, S. C., Orange, A., Hoversten, G. M., Morrison, H. F., 1998, Marine Magnetotellurics for Petroleum Exploration 1. A Seafloor Equipment System: Geophysics, **63**, 816-825.

deGroot-Hedlin, C. and Constable, S. C., 1990, Occam's inversion to generate smooth, two-dimensional models from magnetotelluric data: Geophysics, **55**, 1613-1624.

Edwards, R. N., 1988, Two-dimensional modeling of a towed in-line electric dipole-dipole sea-floor electromagnetic system - the optimum time delay or frequency for target resolution: Geophysics, **53**, 846-853.

Egbert, G.D., 1997, Robust multiple station magnetotelluric data processing: J. Geoph. Intl., **130**, 475-496.

Gamble, T.D., Goubau, W.M., Clarke, J., 1978, Magnetotellurics with a remote magnetic reference: Geophysics, **44**, 53-68.

Filloux, J. H., 1983, Seafloor magnetotelluric soundings in the Mariana island arc area, In: Hayes, Dennis E., editor tectonic and geologic evolution of Southeast Asian seas and islands; Part 2. Washington, DC: Am. Geophys. Union, Geophysical monograph **27**, 255-265

Hoehn, G. L., Warner, B. N., 1960, Magnetotelluric Measurements in the Gulf of Mexico at 20M Ocean Depths: CRC Handbook of Geophysical Exploration at Sea, 397-416.

Hoversten, G. M., Constable, S., Morrison, H. F., 1998, Marine Magnetotellurics for Petroleum Exploration 2. Numerical analysis of subsalt resolution: Geophysics, **63**, 826-840.

Hoversten, G. M., Unsworth, M. 1994, SubSalt Imaging via Seaborne Electromagnetics: Proceedings – Offshore Technology Conference; **26**, 231-240.

Hoversten, G. M., 1992, Seaborne Electromagnetic Subsalt Exploration: EOS, Transactions, AGU; **73**, Suppl., p313.

Mackie, R.L., Livelybrooks, D.W., Madden, T.R., and Larsen, J.C., 1997, A magnetotelluric investigation of the San Andreas fault at Carrizo Plain, California: Geophys. Res. Letters, **24**, 1847-1850.

Mackie, R.L., Madden, T.R., Wannamaker, P.W., 1993, Three-dimensional magnetotelluric modeling using difference equations – Theory and solutions: Geophysics, **58**, 215-226.

Orange, A. S., 1989, Magnetotelluric Exploration for Hydrocarbons: Proc. IEEE, **77**, 287-317.

Petiau, G., and A. Dupis, 1980, Noise, temperature coefficient, and long time stability of electrodes for telluric observations: Geophys. Prospect., **28**, 792-804

Smith, J. T., Booker, J. R., 1988, Rapid Inversion of Two- and Three-Dimensional Magnetotelluric Data: Jou. Geoph. Research, **96**, 3905-3922.

Smith, J. T., Hoversten, G. M., Morrison, H. F., Gasperikova, E., 1999, Sharp Boundary Inversion of 2-D Magnetotelluric Data: Geophys. Prosp., **47**, 469-486.

Vozoff, K., 1972, The Magnetotelluric Method in the Exploration of Sedimentary Basins: Geophysics, **37**, 98-141.

Wannamaker, P.E., Hohmann, G. W., Ward, S. H., 1984, Magnetotelluric responses of three-dimensional bodies in layered earths: Geophysics, **49**, 1517-1533.

Webb, S. C., Constable, S. C., Cox, C. S., Deaton, T. K., 1985, A seafloor electric field instrument. In: Journal of Geomagnetism and Geoelectricity. Tokyo : Society of Terrestrial Magnetism and Electricity of Japan, **37**, 1115-1129

FIGURE CAPTIONS

Figure 1: Electric field noise (lower solid line) collected on adjacent electrodes in 100m water. The spectrum is approximated by a combination of $1/f^2$ electrode noise below 0.2 Hz and an instrument noise floor of 10^{-18} V^2/Hz above 0.2 Hz. The drop at 4 Hz is due to the anti-alias filters, and the peak at 0.1 Hz is associated with gravity (water) waves in the shallow water (is absent in 1000 m water). Signal levels in both 100 m and 1000 m water is shown, as is an estimate of silver-silver chloride electrode taken in the laboratory by Petiau and Dupis (1980). One can obtain electric field levels on a 10-m dipole by dividing all values by 100; thus our instrument noise floor is 10^{-20} $V^2/m^2/Hz$.

Figure 2: Time-series of electric and magnetic field data collected during the Gemini survey, in 1000 m water. Because electric and magnetic data were recorded on separate instruments, electric and magnetic sensors are not necessarily aligned.

Figure 3: 3D view of Gemini Salt seen from the south west. Cube size approzimately 22 by 20 km. Sea floor MT sites shown as red cubes.

Figure 4: Plan view of Apparent resistivities over the Gemini 3D numerical model. a) Zyx Apparent resistivity @ 0.001 Hz, b) Zyx Apparent resistivity @ 0.001Hz, c) Zxy

@.01 Hz, d) Zyx @ 0.01 Hz. The approximate location of the survey line is shown for reference.

Figure 5: Gemini MMT Survey line. Dark shaded area represents salt thickness > 500m. Seafloor site locations used in analysis are shown in black.

Figure 6: Apparent Resistivity rotated so that X is North. ♦ = Z_{xy} apparent resistivity, O = Z_{yx} apparent resistivity.

Figure 7: Phase rotated so that X is North. ♦ = Z_{xy} phase, O = Z_{yx} phase.

Figure 8: Polar impedance diagrams for the 9 seafloor sites, Sites are ordered from South West (Site 5) to North East (Site 19). Rows are constant frequency in Hz (high frequency at top, low frequency at bottom) and columns are constant site location. North is up and east is to the right.

Figure 9: RRI TM mode inversion. Starting model was 0.7 Ω-m halfspace. White line shows salt outline as interpreted from 3-D prestack depth-migrated seismic data. Seawater was not included in the inversion model. Seafloor MT sites shown by red triangles.

Figure 10: NLCG TM mode inversion. Starting model was 0.7 Ω-m halfspace. White line shows salt outline as interpreted from 3-D prestack depth-migrated seismic data. Seafloor MT sites shown by red triangles.

Figure 11: Occam2D TM mode inversion. Starting model was 0.7 Ω-m halfspace. White line shows salt outline as interpreted from 3-D prestack depth-migrated seismic data. No smoothing across blocks at top salt. Seafloor MT sites shown by red triangles.

Figure 12: SBI TM mode inversion, thickness parameterization, of Gemini data. Top of salt boundary location was fixed. Sediment resistivities started at 0.7 Ω-m. Heavy Black lines indicate starting location of base salt and deep resistor. Thin black lines are final SBI boundaries. White line is salt outline from 3-D prestack depth-migrated seismic. Diamonds represent layer boundary nodes. Squares are layer resistivity nodes. Filled symbols are fixed in the inversion. X through a symbol indicates it is linked to the previous node. Circles around symbols indicate constraint as a percentage of its starting value. The base salt was constrained to be within 100% of its starting location.

Figure 13: TM (Z_{xy}) mode Apparent Resistivity rotated so that X is N45E (the line direction). ♦ is observed data, o are calculated from inverse model shown in figure 12

Figure 14: TM (Z_{xy}) Phase rotated so that X is N45E (the line direction). ♦ is observed data, o are calculated from inverse model shown in figure 12.

Figure 15: SBI inverse model, parameterized in terms of layer thickness, of TM model data between 0.001 and 0.1 Hz from 3D numerical model of Gemini with a 10 Ω-m basement at 8km depth.

Figure 16: SBI inverse model, parameterized in terms of layer interface depths, of TM mode data between 0.001 and 0.1 Hz from 3D numerical model of Gemini with a 10 Ω-m basement at 8km depth

Figure 17: Change in apparent resistivity at sites 5 and 11 for 300m change in base salt depth. Initial model taken from SBI inversion of Gemini field data shown in figure 12.

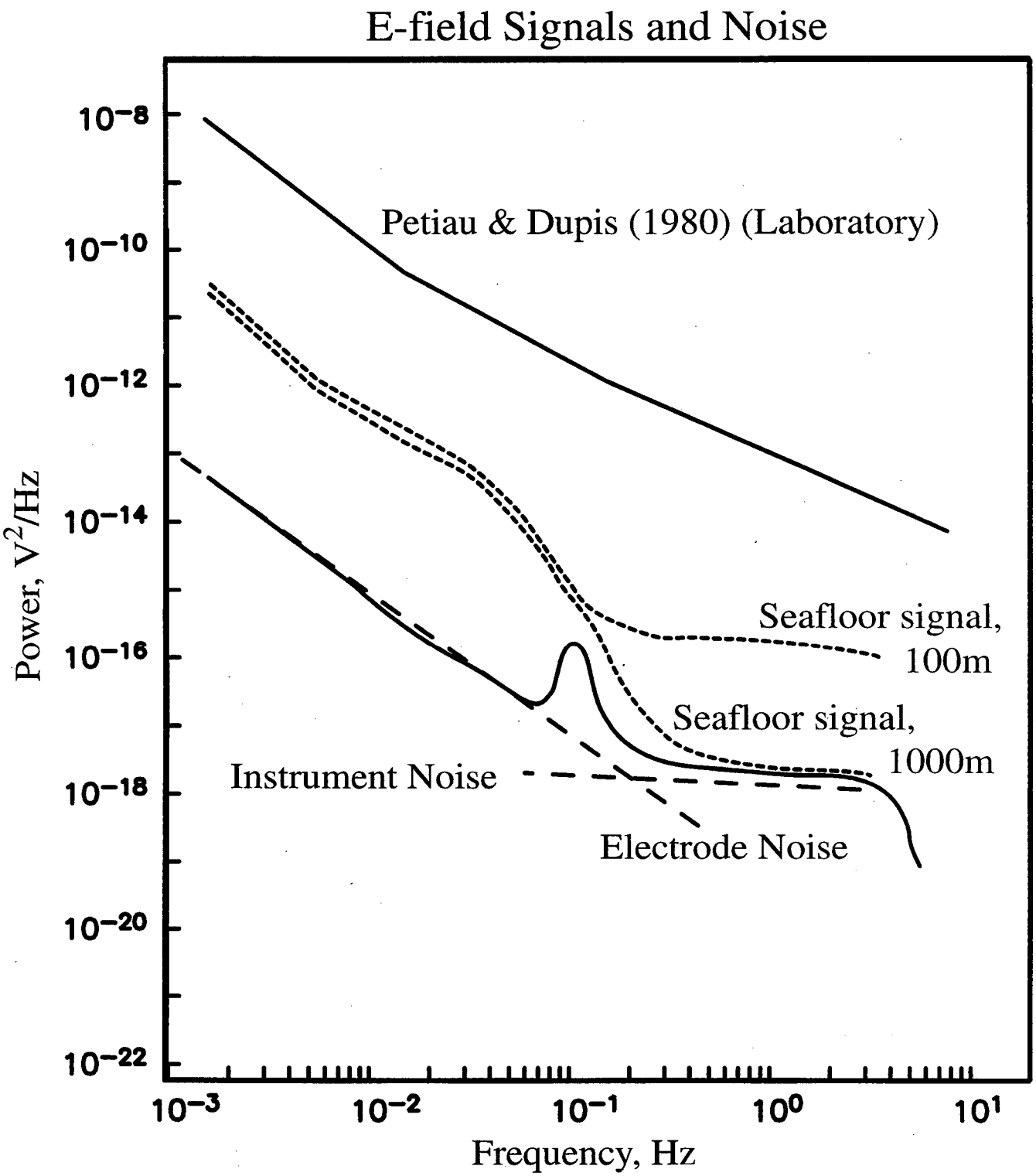
E-field Signals and Noise
Petiau & Dupis (1980) (Laboratory)
Seafloor signal, 100m
Seafloor signal, 1000m
Instrument Noise
Electrode Noise
Power, V²/Hz
Frequency, Hz
10⁻⁸
10⁻¹⁰
10⁻¹²
10⁻¹⁴
10⁻¹⁶
10⁻¹⁸
10⁻²⁰
10⁻²²
10⁻³
10⁻²
10⁻¹
10⁰
10¹

FIGURE 1

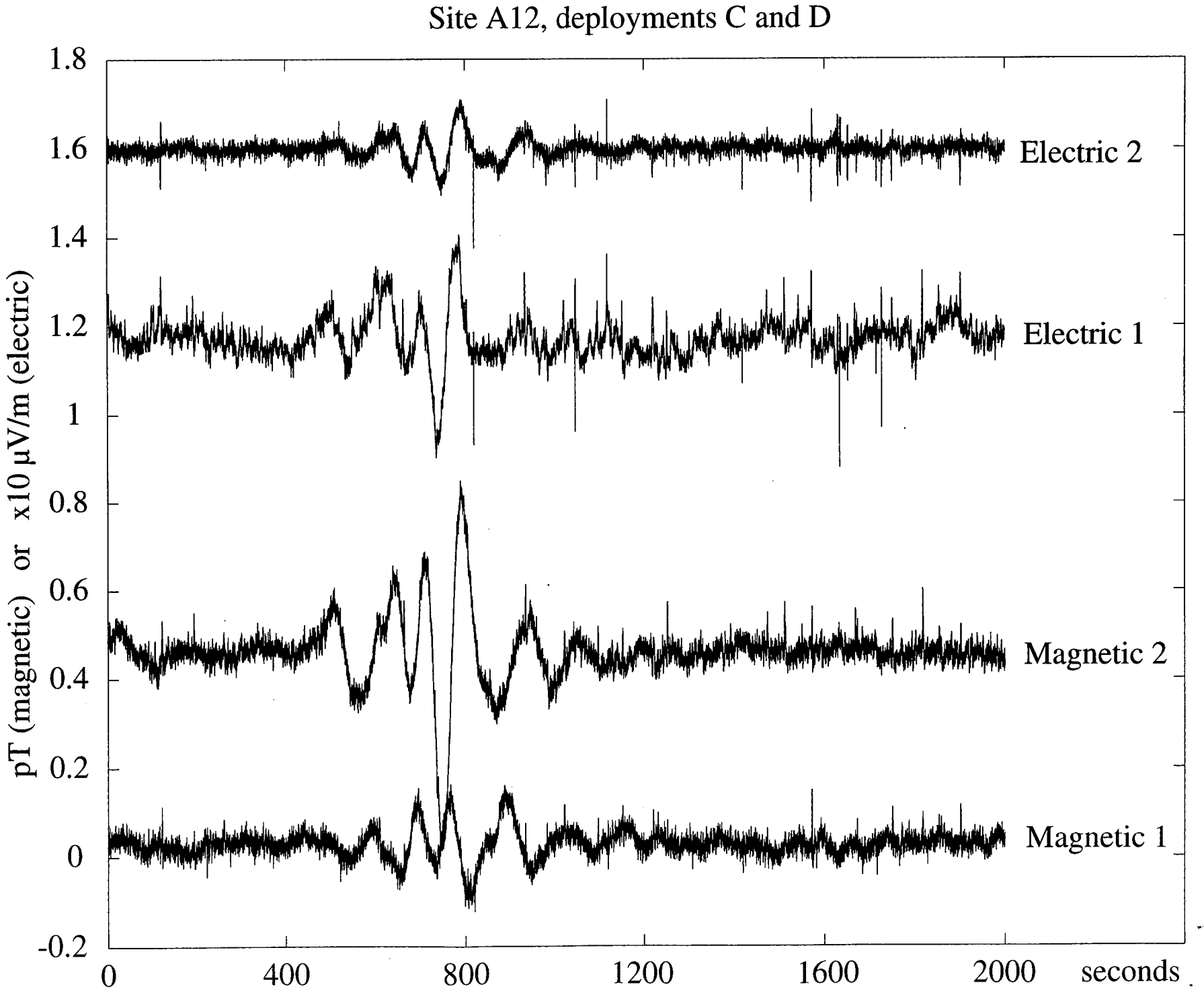
Site A12, deployments C and D
pT (magnetic) or x10 μV/m (electric)
1.8
1.6
1.4
1.2
1
0.8
0.6
0.4
0.2
0
-0.2
0
400
800
1200
1600
2000
seconds
Electric 2
Electric 1
Magnetic 2
Magnetic 1

FIGURE 2

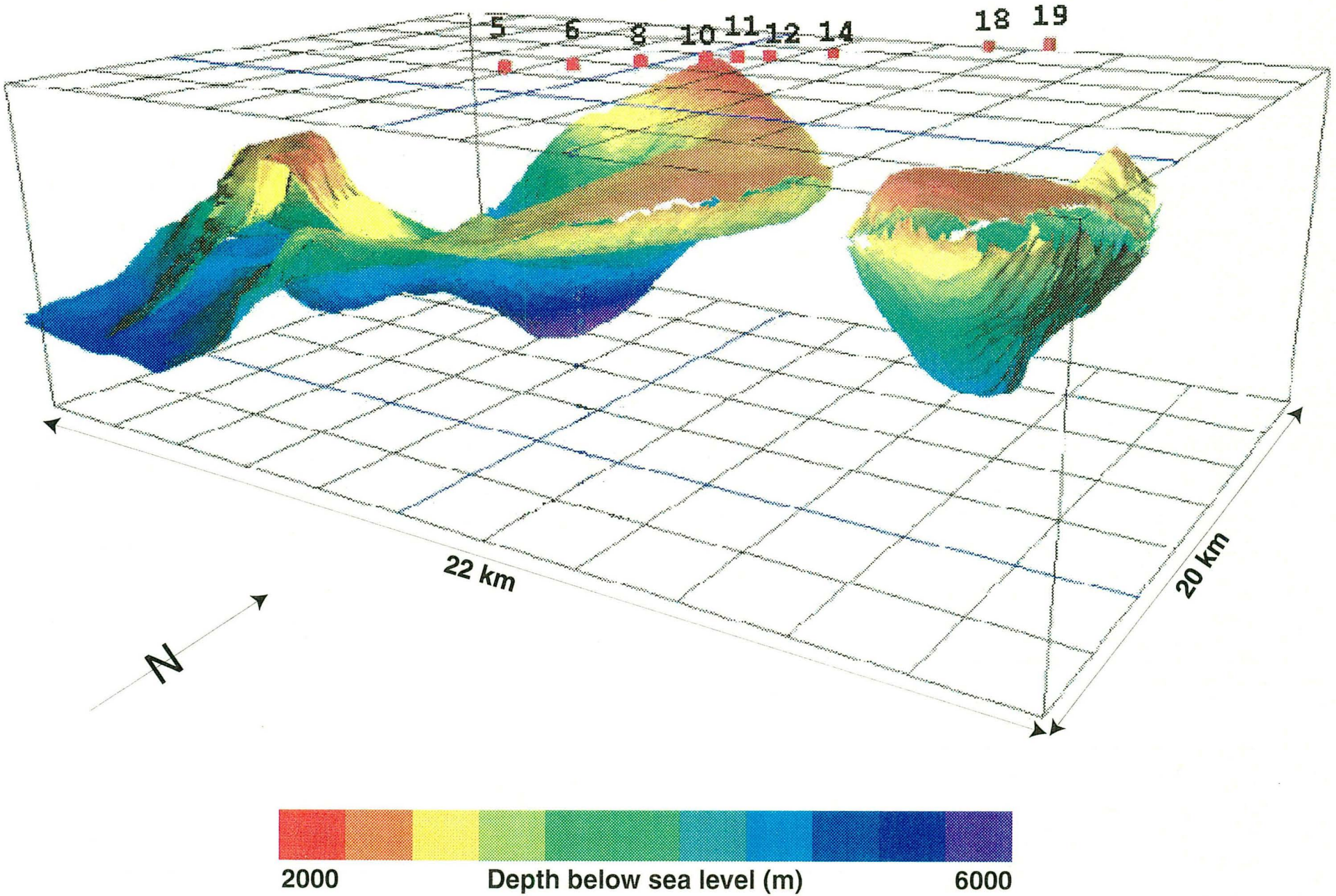
5
6
8
10
11
12
14
18
19
22 km
20 km
N
2000
Depth below sea level (m)
6000

FIGURE 3

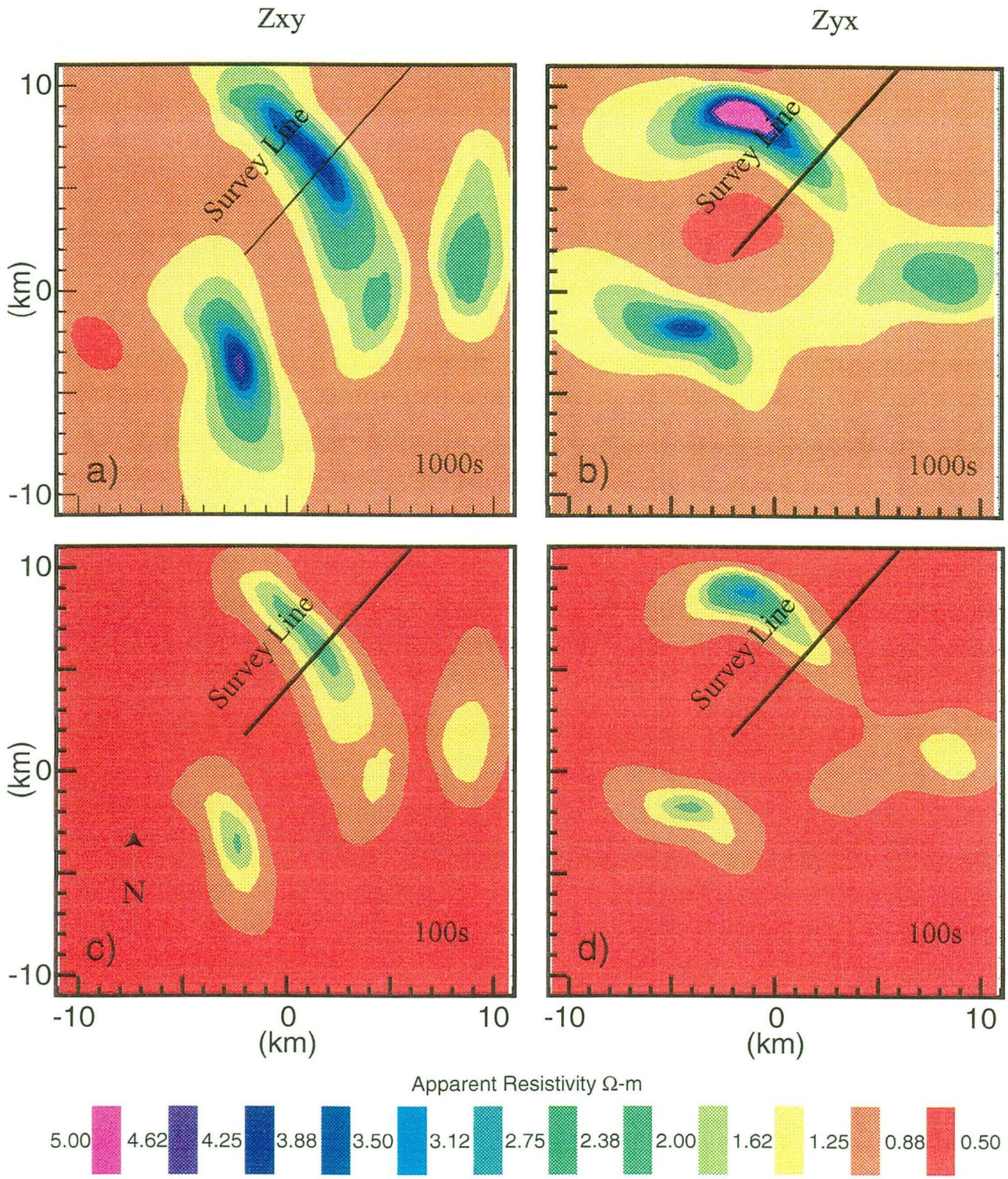
Zxy
Zyx
Survey Line
a)
1000s
b)
c)
100s
d)
N
(km)
10
0
-10
Apparent Resistivity Ω-m
5.00
4.62
4.25
3.88
3.50
3.12
2.75
2.38
2.00
1.62
1.25
0.88
0.50

FIGURE 4

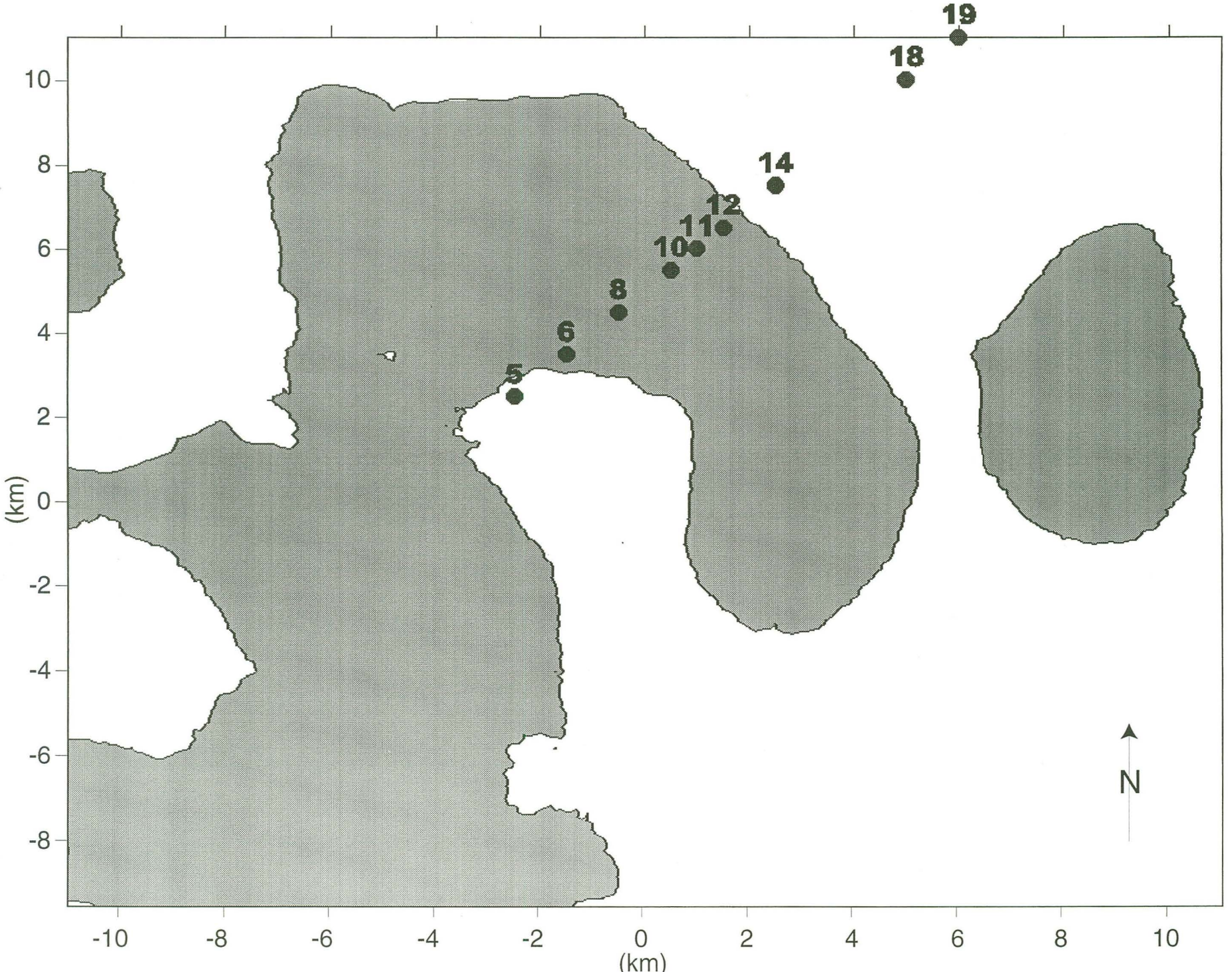

FIGURE 5

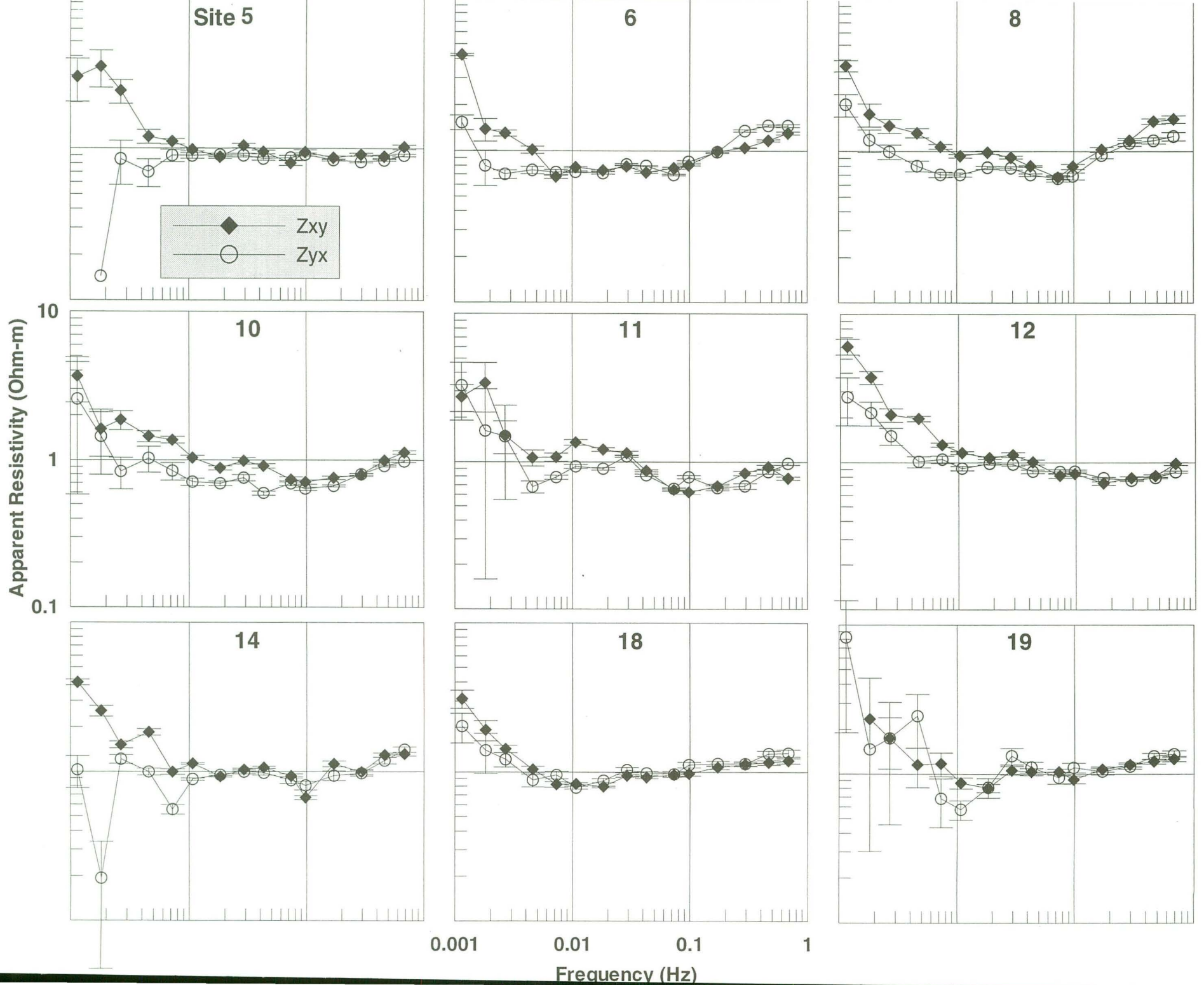
Site 5
6
8
10
11
12
14
18
19
Zxy
Zyx
Apparent Resistivity (Ohm-m)
10
1
0.1
0.001
0.01
0.1
1
Frequency (Hz)

FIGURE 6

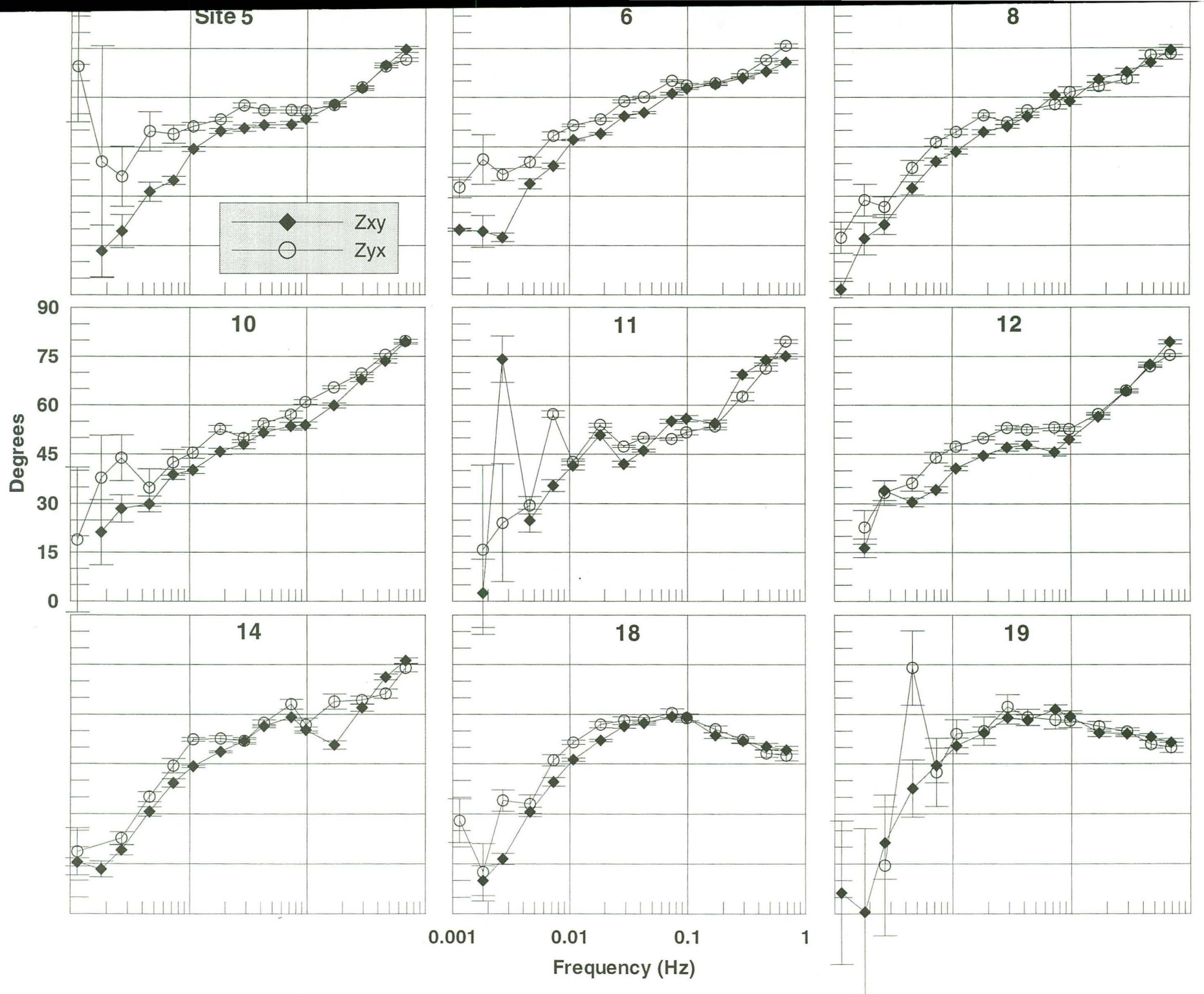
Site 5
6
8
10
11
12
14
18
19
Zxy
Zyx
Degrees
90
75
60
45
30
15
0
0.001
0.01
0.1
1
Frequency (Hz)

FIGURE 7

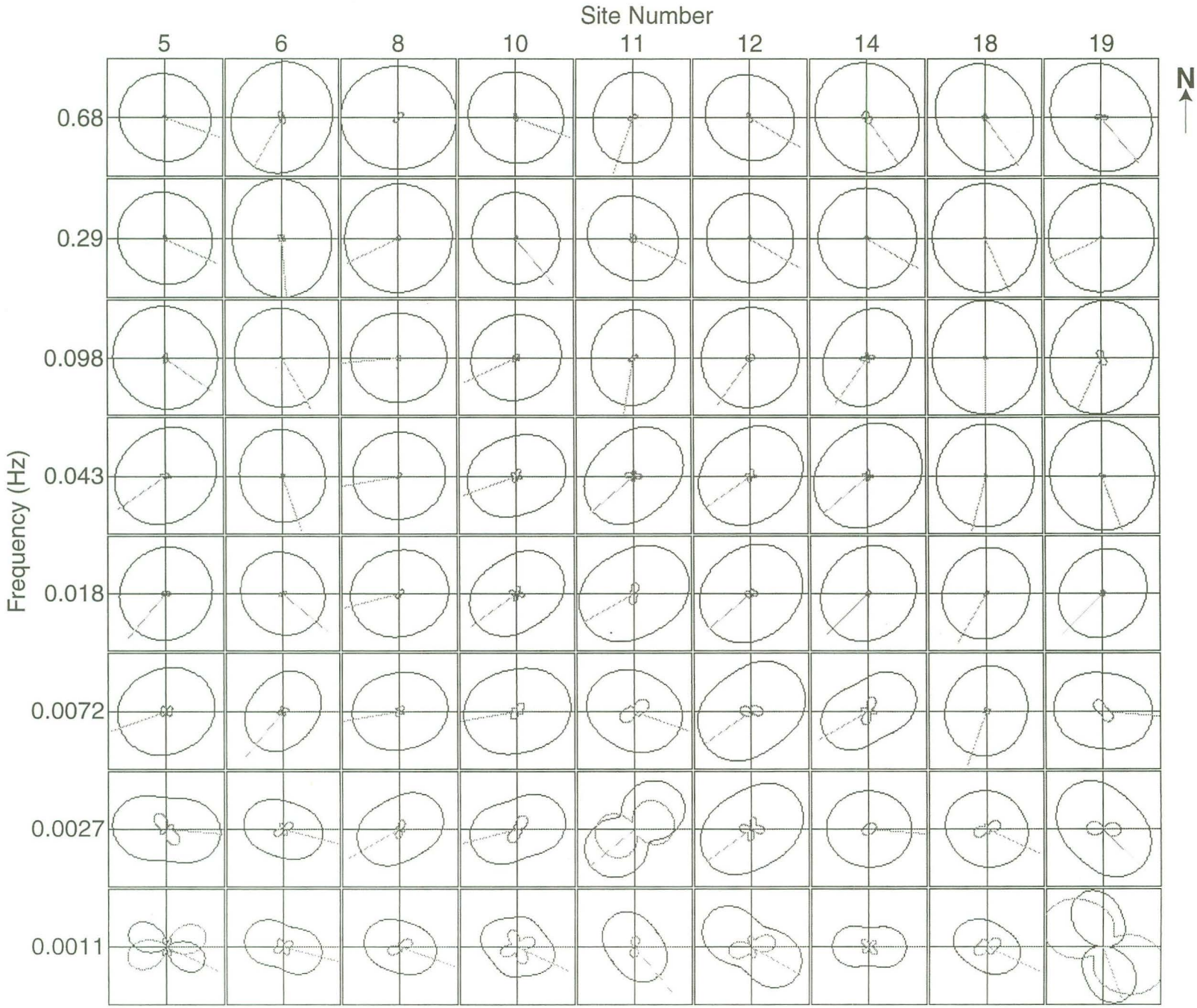
Site Number
5
6
8
10
11
12
14
18
19
N
Frequency (Hz)
0.68
0.29
0.098
0.043
0.018
0.0072
0.0027
0.0011

FIGURE 8

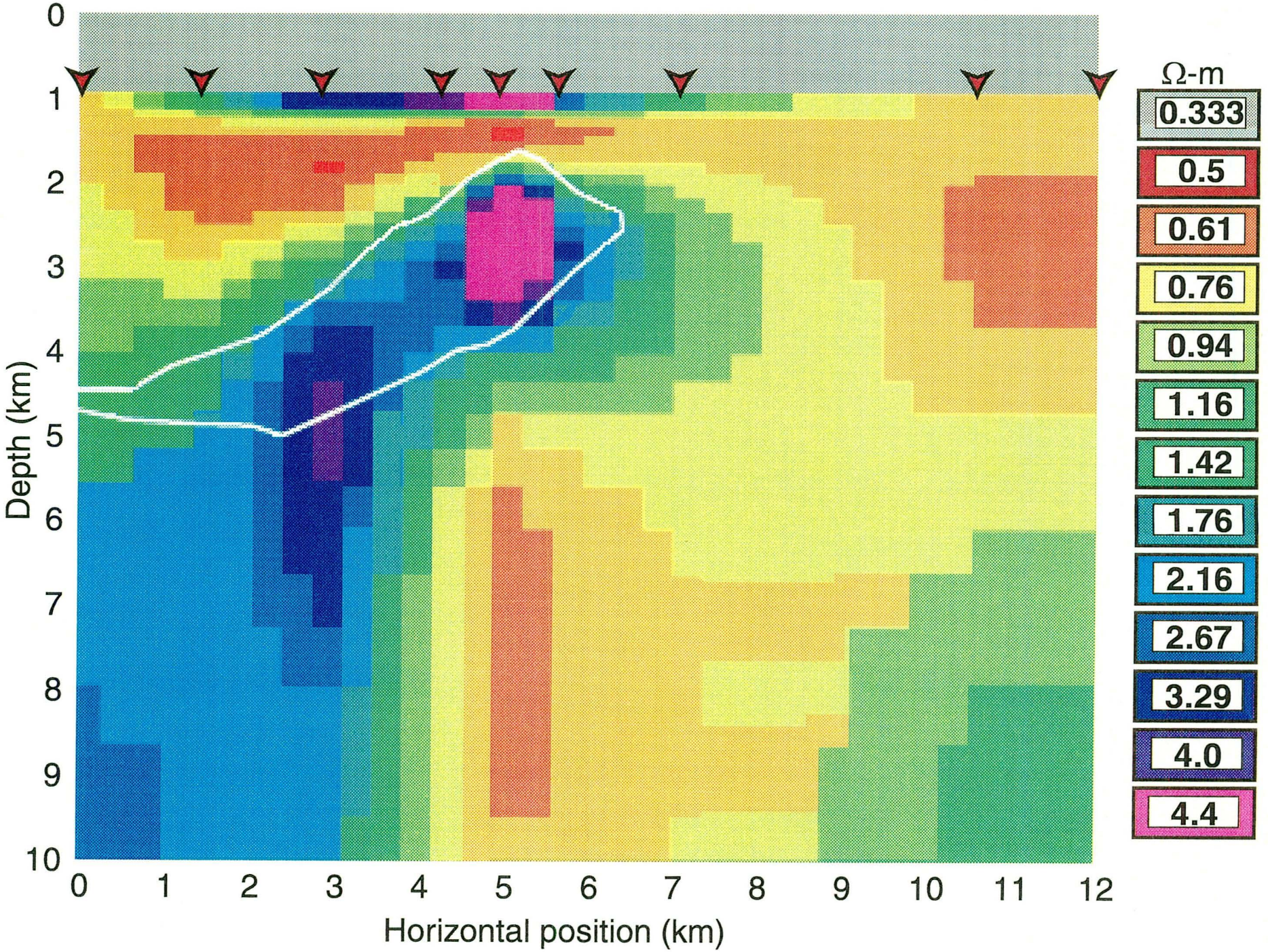
Depth (km)
0
1
2
3
4
5
6
7
8
9
10
Horizontal position (km)
0
1
2
3
4
5
6
7
8
9
10
11
12
Ω-m
0.333
0.5
0.61
0.76
0.94
1.16
1.42
1.76
2.16
2.67
3.29
4.0
4.4

FIGURE 9

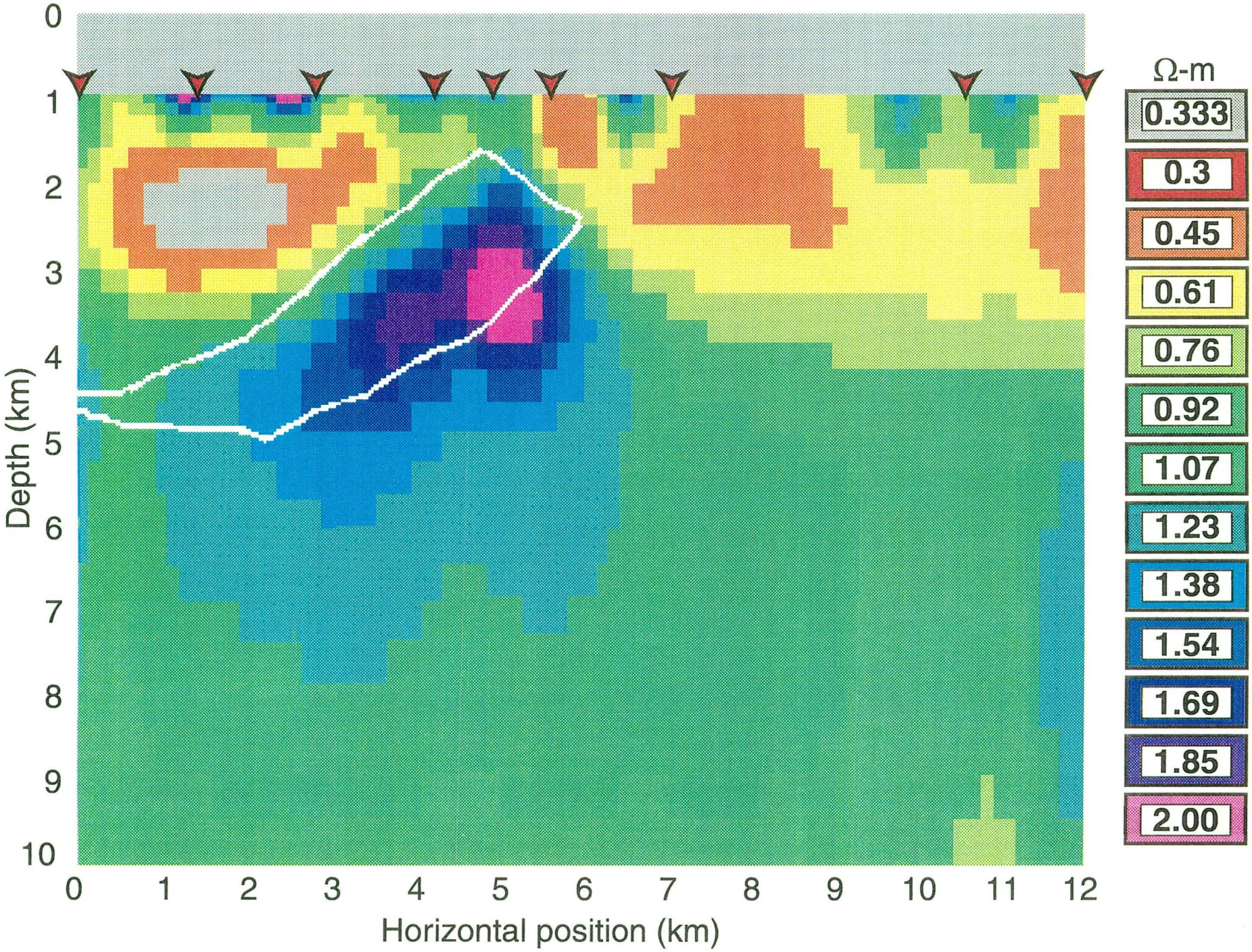
Depth (km)
0
1
2
3
4
5
6
7
8
9
10
Horizontal position (km)
0
1
2
3
4
5
6
7
8
9
10
11
12
Ω-m
0.333
0.3
0.45
0.61
0.76
0.92
1.07
1.23
1.38
1.54
1.69
1.85
2.00

FIGURE 16

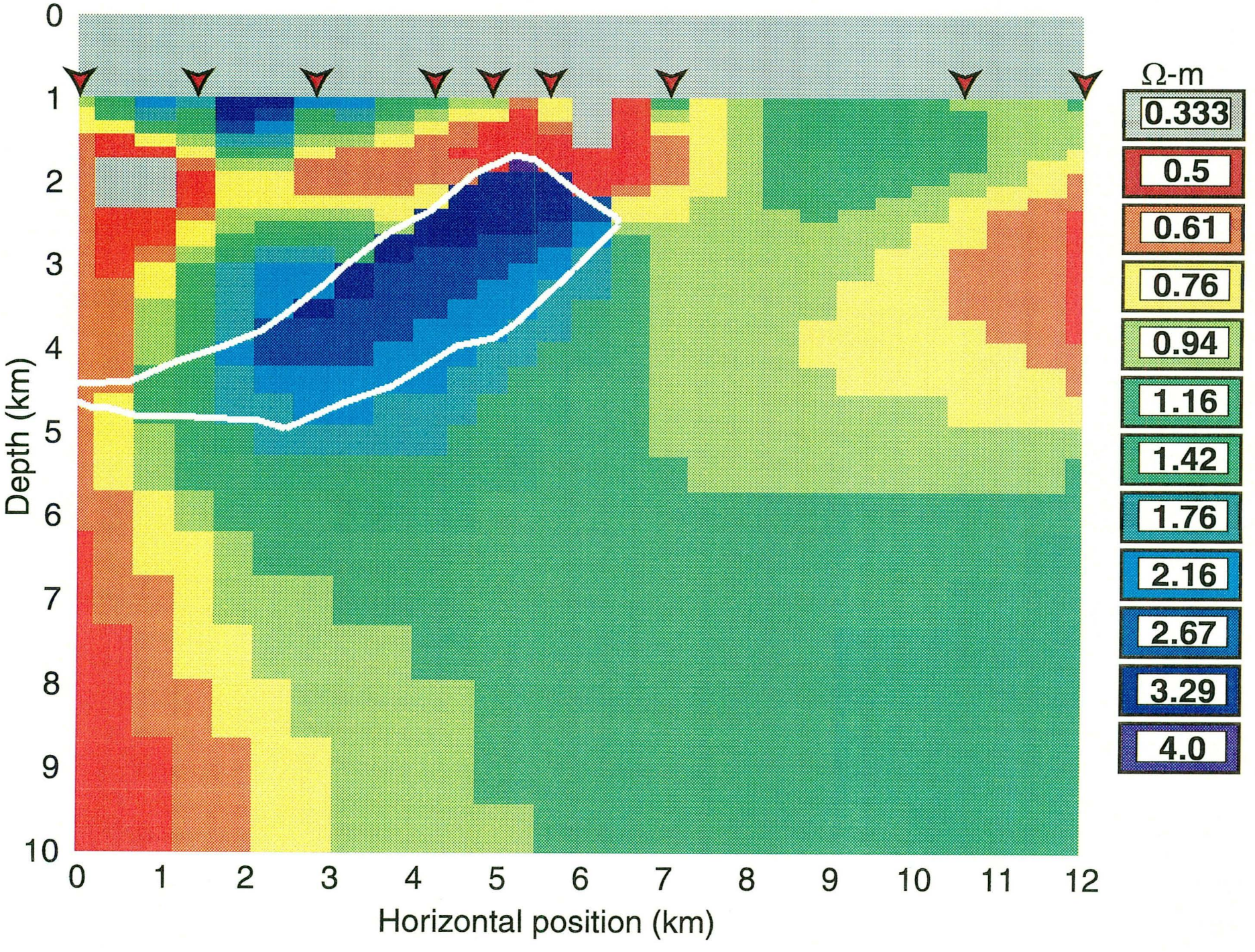
Depth (km)
0
1
2
3
4
5
6
7
8
9
10
Horizontal position (km)
0
1
2
3
4
5
6
7
8
9
10
11
12
Ω-m
0.333
0.5
0.61
0.76
0.94
1.16
1.42
1.76
2.16
2.67
3.29
4.0

FIGURE 11

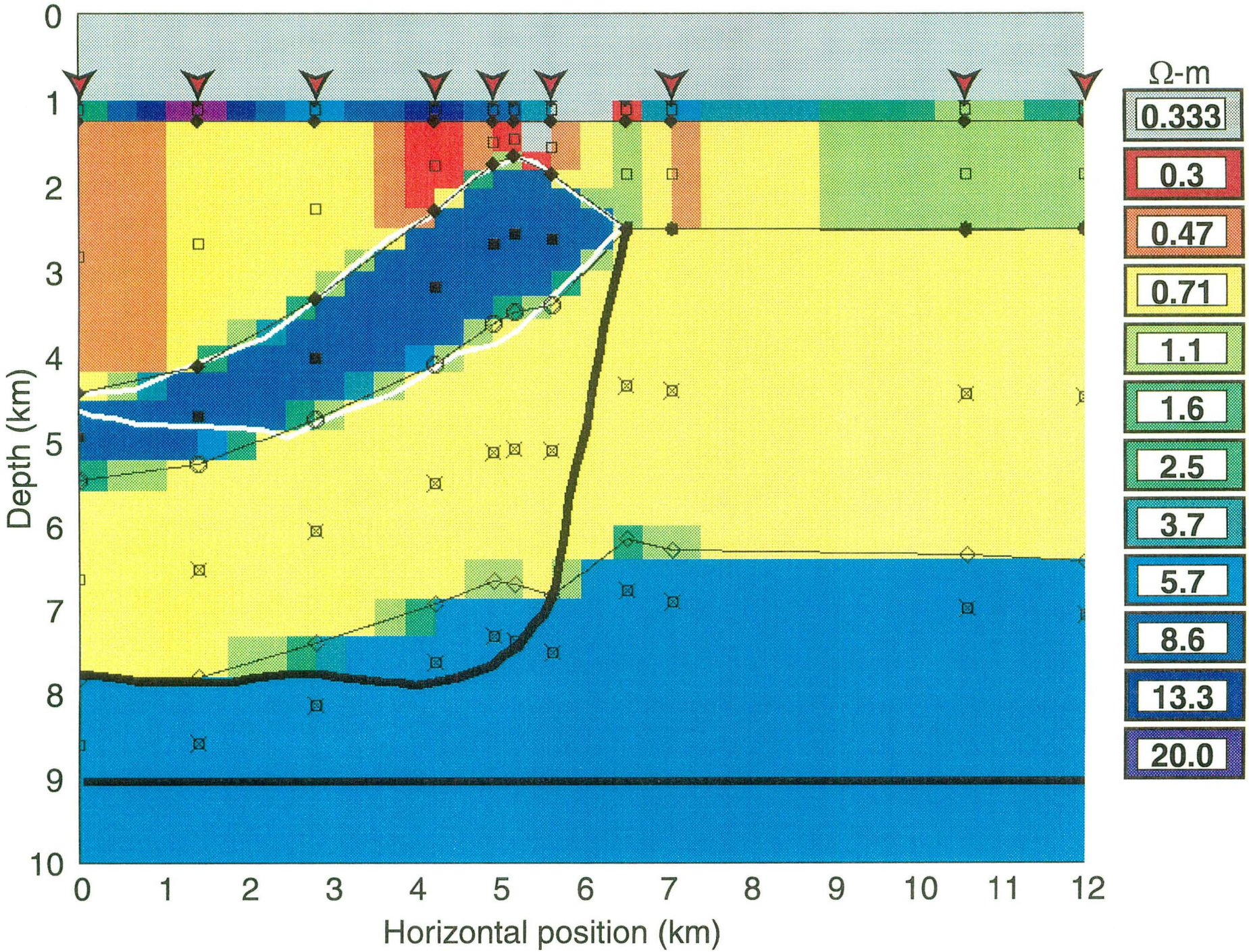
Depth (km)
Horizontal position (km)
Ω-m
0.333
0.3
0.47
0.71
1.1
1.6
2.5
3.7
5.7
8.6
13.3
20.0

FIGURE 1

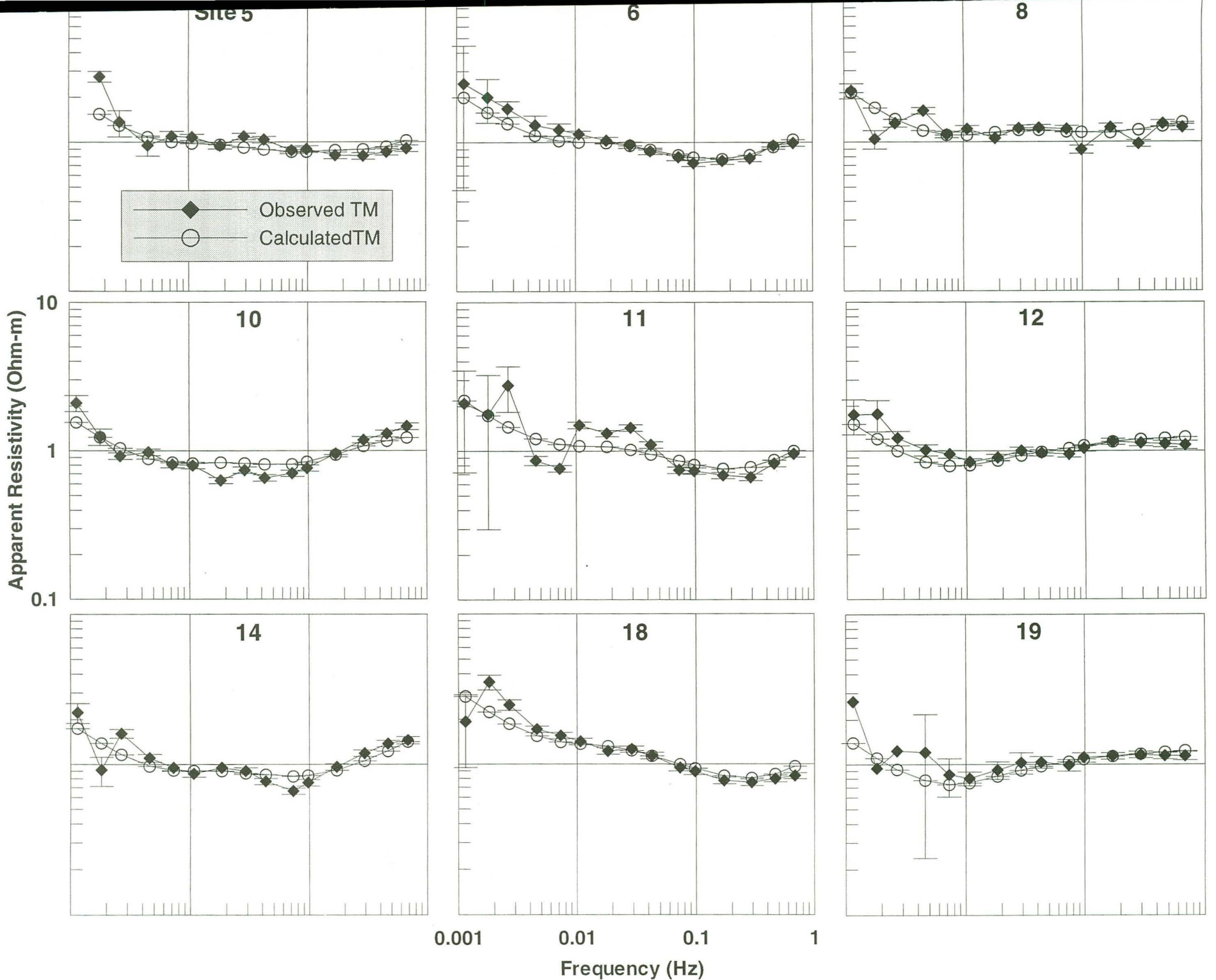
Site 5
6
8
10
11
12
14
18
19
Observed TM
CalculatedTM
Apparent Resistivity (Ohm-m)
10
1
0.1
0.001
0.01
0.1
1
Frequency (Hz)

FIGURE 13

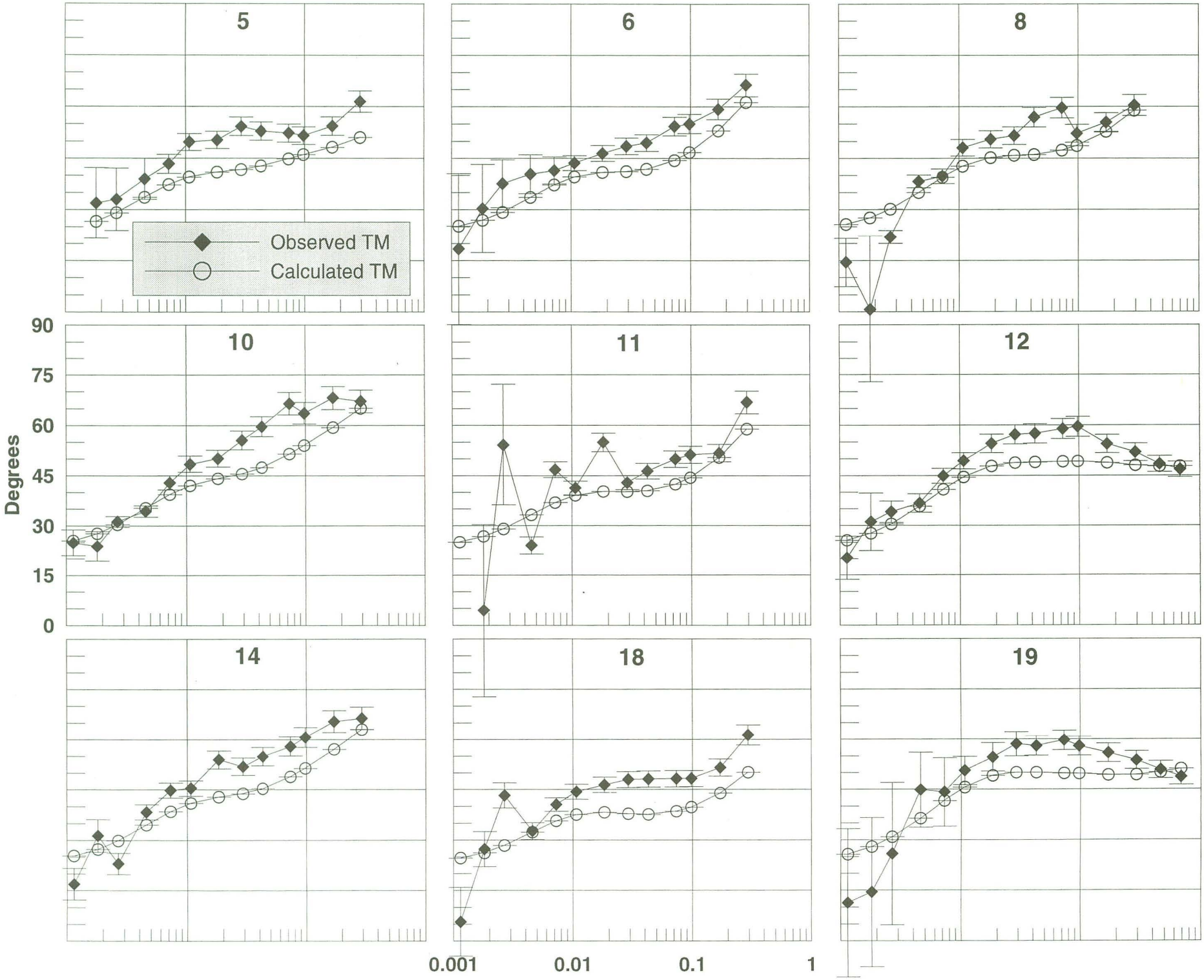
5
6
8
10
11
12
14
18
19
Observed TM
Calculated TM
Degrees
90
75
60
45
30
15
0
0.001
0.01
0.1
1

FIGURE 19

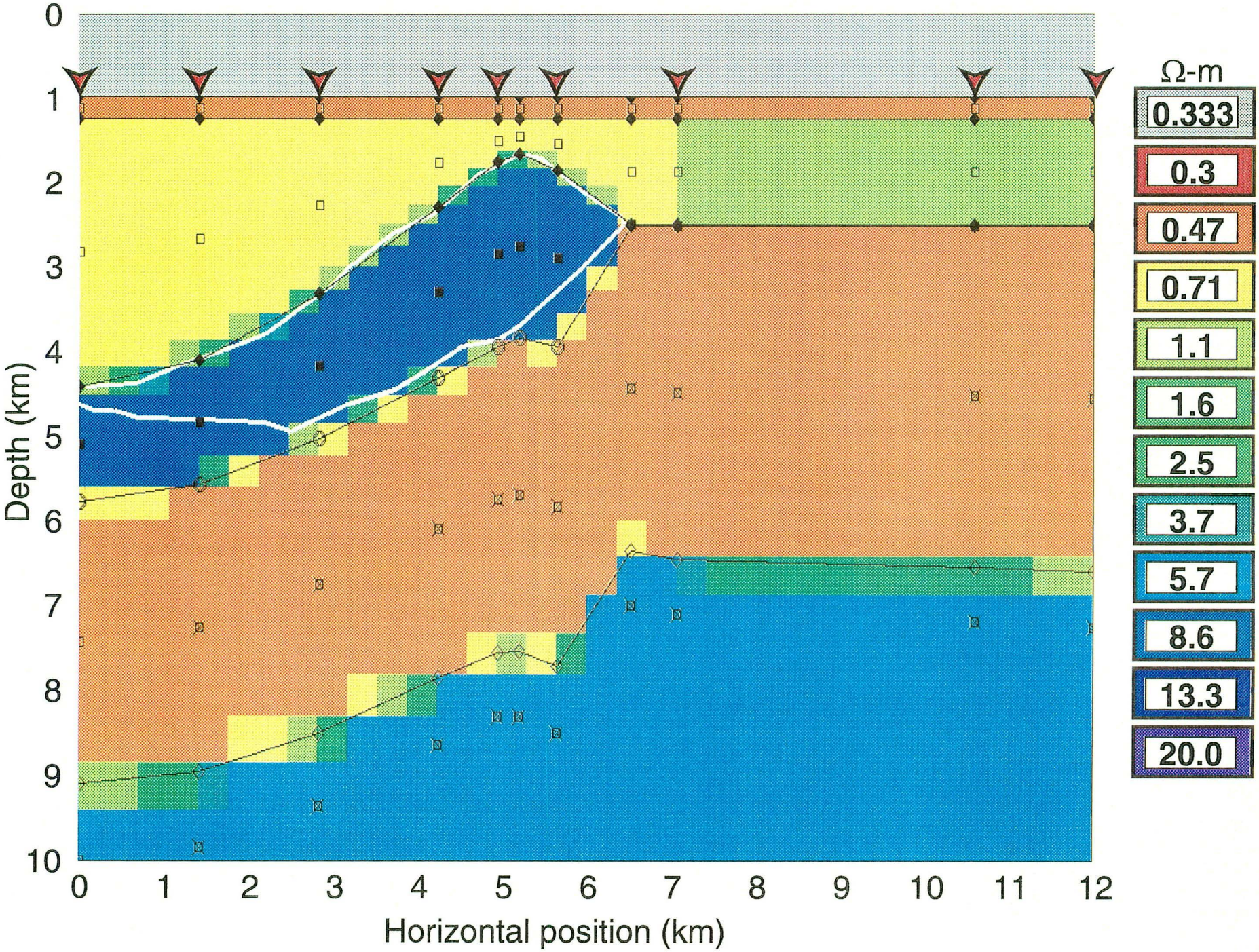
Depth (km)
Horizontal position (km)
0
1
2
3
4
5
6
7
8
9
10
11
12
Ω-m
0.333
0.3
0.47
0.71
1.1
1.6
2.5
3.7
5.7
8.6
13.3
20.0

FIGURE 15

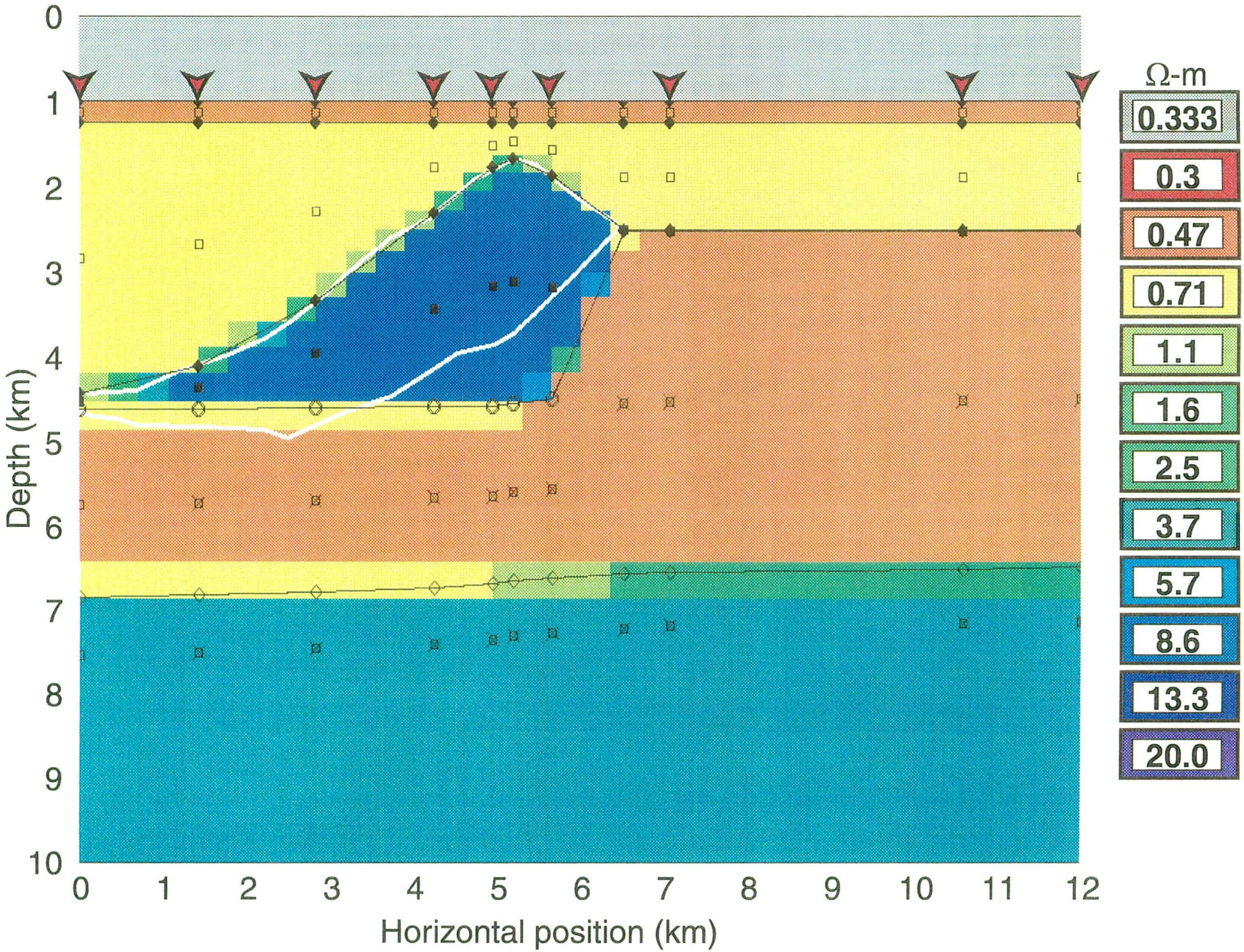
Depth (km)
0
1
2
3
4
5
6
7
8
9
10
Horizontal position (km)
0
1
2
3
4
5
6
7
8
9
10
11
12
Ω-m
0.333
0.3
0.47
0.71
1.1
1.6
2.5
3.7
5.7
8.6
13.3
20.0

FIGURE 1

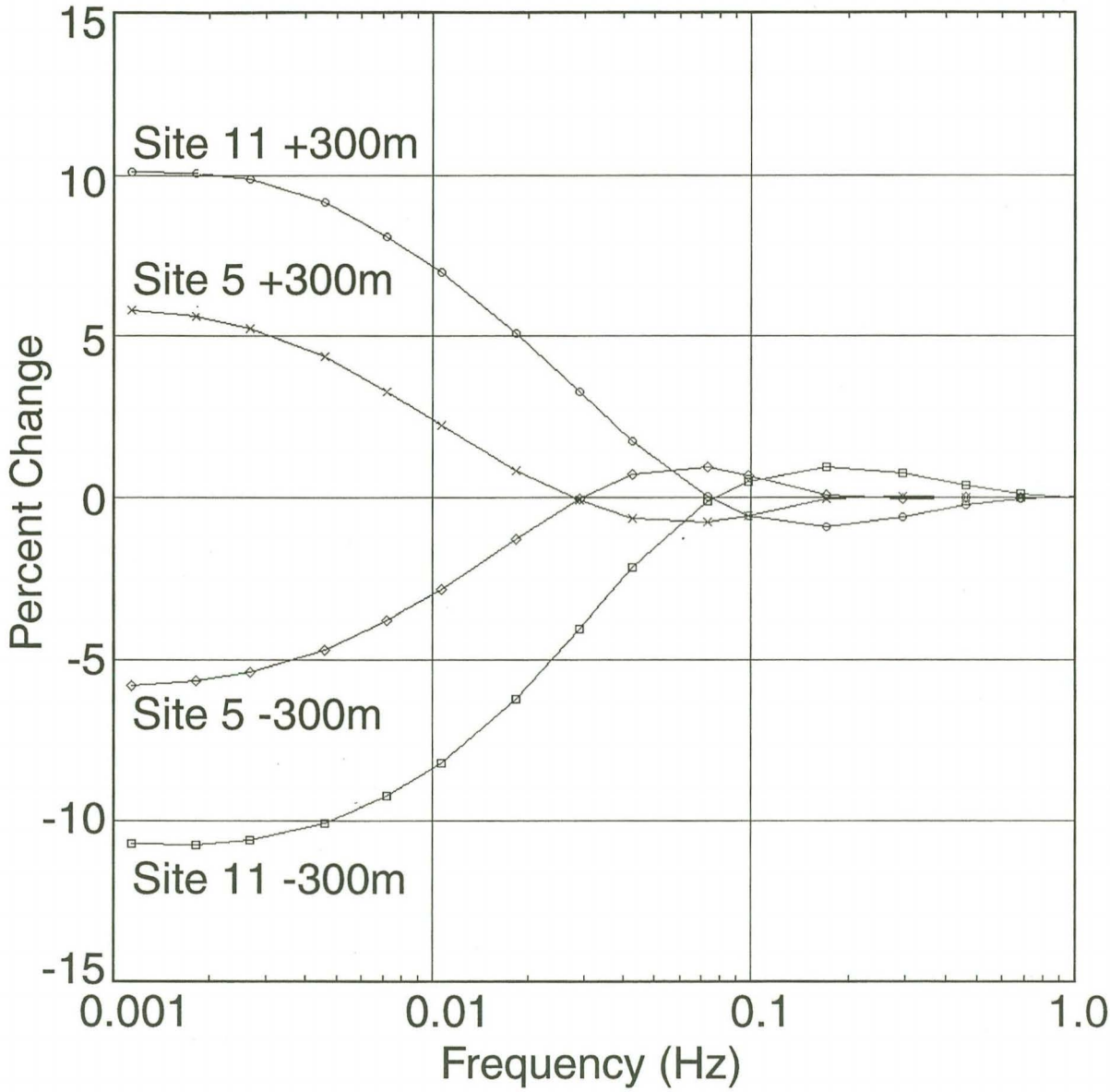
15
10
5
0
-5
-10
-15
Percent Change
Site 11 +300m
Site 5 +300m
Site 5 -300m
Site 11 -300m
0.001
0.01
0.1
1.0
Frequency (Hz)

FIGURE 17

Ernest Orlando Lawrence Berkeley National Laboratory
One Cyclotron Road | Berkeley, California 94720

Prepared for the U.S. Department of Energy under Contract No. DE-AC03-76SF00098